# A VARIATIONAL APPROACH TO BLENDING BASED ON WARPING FOR NON-OVERLAPPED IMAGES

By

**Chang-Ock Lee**

**Kiwan Jeon**

**Youngsoo Ha**

and

**Jooyoung Hahn**

**IMA Preprint Series # 2076**

( November 2005 )

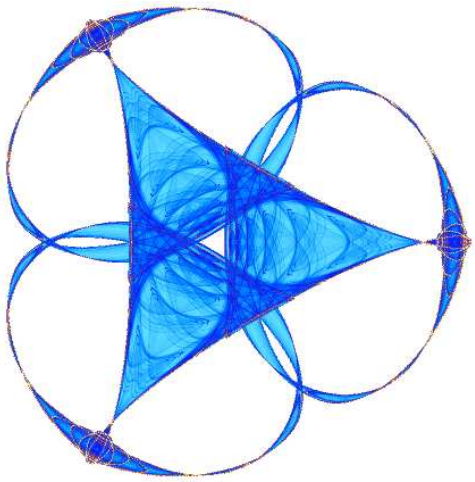

INSTITUTE FOR MATHEMATICS AND ITS APPLICATIONS

UNIVERSITY OF MINNESOTA
400 Lind Hall
207 Church Street S.E.
Minneapolis, Minnesota 55455–0436

Phone: 612/624-6066 Fax: 612/626-7370
URL: http://www.ima.umn.edu

# A Variational Approach to Blending Based on Warping for Non-overlapped Images*

Chang-Ock Lee†, Kiwan Jeon‡, Youngsoo Ha§, Jooyoung Hahn¶
Division of Applied Mathematics, KAIST, Daejeon, 305-701, Korea

**Abstract**

This paper presents a new model for image blending based on warping. The model is represented by partial differential equations (PDEs) and gives a sequence of images, which has the properties of both blending of image intensities and warping of image shapes. We modified the energy functional in [1] in order to adapt the idea of the shape warping to the image blending. The PDEs from the proposed energy functional cover not only overlapped images but also non-overlapped ones.

Key words: Image blending, warping, variational approach

## 1 Introduction

A general image blending method is the linear interpolation of intensity values between two images, namely source and target. This method is easy to generate a sequence of images. The sequence, however, has a drawback that the image in the source fades out and the image in the target fades in except on common regions. The image blending method in [2] is based on partial differential equations (PDEs) by minimizing the area of the symmetric difference in each intensity level. In the paper, to create a blending sequence, the method makes an intermediate image as evolving the source and the target simultaneously. The level set approach in [2] does not have unreasonable disappearing and appearing effects when two images have an overlapping region. Unfortunately, if the source and target images are non-overlapped, this method gives the same weak point as the general image blending case.

Object warping method is a possible solution to the problem for the non-overlapping case. Warping is one of the important issues of computer vision: pattern recognition, animation and medical image. One of the general warping method is based on landmark or

*This work was partially supported by KRF-2002-070-C00004 and KOSEF R01-2000-00008.

†E-mail: colee@amath.kaist.ac.kr. Supported in part by the Institute for Mathematics and its Applications with funds provided by the National Science Foundation.

‡E-mail: piewani@hotmail.com

§E-mail: young@amath.kaist.ac.kr

¶E-mail: jyhahn76@amath.kaist.ac.kr

control point-matching [3–6]. This method is popular and gives good results, however, it is not appropriate to our problem because it is based on the matching of the landmark or control points given by users and we want to develop an automatic image blending algorithm depending on the given image intensities. Another is the minimization of some measure between shape objects, which is made under the appropriate constraint; for example, distance or shape intensity profile, etc. See the references [1, 7–11]. Among them, Liao *et al.* [1] introduced a noble model of shape warping for the non-overlapping case, which comes from the object matching problem in medical image processing. The method was formulated by the level set function [12, 13] having zero level at the shape boundary. Even though the model gives a possibility for solving the non-overlapping matching problem, it also needs the boundary information given by users and causes tadpole shapes in the sequence of images since this method just tries to make a shape from the source be the target one.

In this paper, we present a new model for the image blending based on the warping. The model is described by PDEs from the energy functional in [1], which is modified to extend the shape warping idea to the image blending. To get more smooth shapes without the tadpole phenomenon, we suggest two deformation fields for the source and the target. Then the model gives a sequence of images, which has the properties of both blending of image intensities and warping of image shapes. Furthermore, it covers not only overlapped images but also non-overlapped ones.

This paper consists of following sections. In Section 2, we design an energy functional which enables to make an image sequence for non-overlapped shapes, and use Euler-Lagrange method and gradient-decent method to derive the PDEs. Section 3 is organized into two parts. At first we explain an algorithm for generating a blending sequence based on warping by using the PDEs in the previous section. Next, we consider the methods of interpolation to create the sequence of images and comment some points to make a better result. Before the conclusion, we illustrate six examples using the synthetic and real images in Section 4.

## 2 Variational Formulations

In this section, we introduce an energy functional which gives two deformation fields for non-overlapped shapes. Given two shapes $S$ and $T$ in the domain $\Omega$, so called the source and the target, respectively, we define $\phi(x)$ and $\psi(x)$, $x \in \mathbf{R}^2$, to be signed distance functions having zero values on each shape boundary. To match two shapes, we find two deformation fields $u(x)$ and $v(x) \in \mathbf{R}^2$ for the source and the target, respectively, by minimizing the energy functional

$$\begin{aligned} E_1(u,\, v) = \int_\Omega \max\{|\phi(x-u)|, |\psi(x-v)|\}\{\mathcal{H}(\psi(x-v)) \\ [1-\mathcal{H}(\phi(x-u))] + \mathcal{H}(\phi(x-u))[1-\mathcal{H}(\psi(x-v))]\} dx\,, \end{aligned} \tag{2.1}$$

where $\mathcal{H}(x)$ is the Heaviside function. If only one deformation field evolving from the source to the target is used, it may cause the large distortion of shape in the image sequence. This

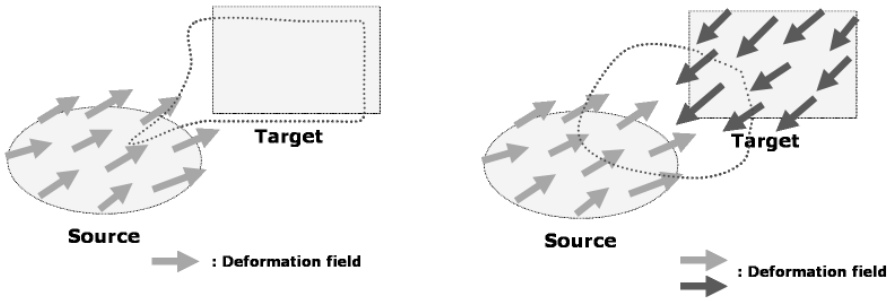


(a) (b)

Figure 1: Two deformation fields have smaller distortion than only one deformation field does. The dotted line in (a) is the shape from the source. The dotted line in (b) is an intermediate shape from the source and the target.

hinders the mobility of shape in source, which should become identical to the shape in target; see Figure 1-(a). In order to reduce the distortion, we use two deformation fields $u(x)$ from the source and $v(x)$ from the target. That is, two vector fields make the movement of both the source and the target and eventually two shapes become identical with less distortion, which we call the intermediate shape; see Figure 1-(b).

The key ingredient of the energy functional (2.1) is the distance information between the source and the target which are arbitrarily given. More precisely, for a non-overlapping case the functional does the integration of the distance functions which are zero on the boundary of one shape over the other shape area. In the shape warping [1], since the shapes of the source and the target are known, the signed distance functions which are positive inside the shapes are used in the energy functional. In our algorithm for the image blending, we define signed distance functions by assigning positive values to the region where the intensity is higher. Hence it is not possible to distinguish between the inside and the outside of shapes by the signs of signed distance functions. Therefore, the integration is not performed inside the target and the source. One possible way to solve this problem is using maximum of distances to the source and the target from the region where the signed distance is positive. Obviously, we see that for the non-overlapping case, if a point is inside the source or the target, then the distance between the point and the other shape is lager than one between the point and the boundary of its own shape. Therefore, we have the deformation fields which minimize the distance between the source and the target by minimizing the energy functional (2.1).

Now, we apply the Euler-Lagrange method to (2.1) with respect to $u$. Then we get the Euler-Lagrange equation

$$-F_1(u, v) = 0,$$

$$F_1(u,v) = \begin{cases} |\psi(x-v)|[1-2\mathcal{H}(\psi(x-v))]\delta(\phi(x-u))\,\nabla\phi(x-u) & \text{in } \tilde{\Omega}_s, \\ \\ \{|\phi(x-u)|[1-2\mathcal{H}(\psi(x-v))]\delta(\phi(x-u)) & \\ \quad +\text{sgn}(\phi(x-u))[\mathcal{H}(\psi(x-v))(1-\mathcal{H}(\phi(x-u))) & \text{elsewhere,} \\ \quad +\mathcal{H}(\phi(x-u))(1-\mathcal{H}(\psi(x-v)))]\}\,\nabla\phi(x-u) & \end{cases}$$

where $\tilde{\Omega}_s := \{\, x : |\psi(x-v)| \geq |\phi(x-u)|\}$. The function $\delta(x)$ denotes the Dirac delta funtion as the derivative of the Heaviside function in the distribution sense. In the same manner with respect to $v$, we obtain the Euler-Lagrange equation:

$$-G_1(u,v) = 0,$$

$$G_1(u,v) = \begin{cases} |\phi(x-u)|[1-2\mathcal{H}(\phi(x-u))]\delta(\psi(x-v))\,\nabla\psi(x-v) & \text{in } \tilde{\Omega}_t, \\ \\ \{|\psi(x-v)|[1-2\mathcal{H}(\phi(x-u))]\delta(\psi(x-v)) & \\ \quad +\text{sgn}(\psi(x-v))[\mathcal{H}(\phi(x-u))(1-\mathcal{H}(\psi(x-v))) & \text{elsewhere,} \\ \quad +\mathcal{H}(\psi(x-v))(1-\mathcal{H}(\phi(x-u)))]\}\,\nabla\psi(x-v) & \end{cases}$$

where $\tilde{\Omega}_t := \{\, x : |\phi(x-u)| \geq |\psi(x-v)|\}$.

If the shapes are overlapped during the evolution of the deformation fields, we use a different energy functional in order to satisfy the shape matching condition in the Section 3.4. The functional $E_2$ is the area of the symmetric difference of the two regions with a positive value of the signed distance function, suggested by Whitaker [2] and Liao *et al.* [1]. That is,

$$\begin{aligned} E_2(u,v) = &\int_\Omega \mathcal{H}(\psi(x-v))[1-\mathcal{H}(\phi(x-u))]\;dx \\ &+ \int_\Omega \mathcal{H}(\phi(x-u))[1-\mathcal{H}(\psi(x-v))]\;dx\,. \end{aligned} \tag{2.2}$$

In the same way as the non-overlapping case, we obtain the Euler-Lagrange equations corresponding to the overlapping case:

$$\begin{aligned} F_2(u,v) &= -[1-2\mathcal{H}(\psi(x-v))]\delta(\phi(x-u))\nabla\phi(x-u) = 0, \\ G_2(u,v) &= -[1-2\mathcal{H}(\phi(x-u))]\delta(\psi(x-v))\nabla\psi(x-v) = 0, \end{aligned}$$

for $u$ and $v$, respectively.

The deformation fields from the above equations are not smooth enough to obtain an image sequence with natural moving. In this paper, we use the regularization $\mathcal{R}(u,v)$, proposed by Horn and Shunck [14], to overcome this drawback:

$$\mathcal{R}(u,v) = \frac{1}{2}\sum_{i=1}^{2}\left\{\|\nabla u^i\|_{L_2}^2 + \|\nabla v^i\|_{L_2}^2\right\} \tag{2.3}$$

where $u^i$ and $v^i$ are components of $u$ and $v$, respectively. Adding the regularization term (2.3) multiplied by the weight factor $\alpha$ to the energy functional (2.1) and (2.2), we obtain the penalized energy functionals

$$E_i(u,\ v) + \alpha \mathcal{R}(u, v)\ ,\ i = 1, 2.$$

We apply the Euler-Lagrange method to the above penalized energy functional with respect to $u$ and $v$. Then we get

$$\begin{aligned} -\alpha \Delta u - F_i(u, v) &= 0 \\ -\alpha \Delta v - G_i(u, v) &= 0 \end{aligned}$$

for $i = 1, 2$.

One method to solve these equations is the gradient descent method. Then we finally formalize a system of PDEs for the deformation fields:

$$\begin{aligned} \frac{\partial u(x,t)}{\partial t} &= \alpha \Delta u + F_i(u, v) \\ \frac{\partial v(x,t)}{\partial t} &= \alpha \Delta v + G_i(u, v) \end{aligned} \tag{2.4}$$

for $i = 1, 2$.

# 3 Image Blending based on Warping

We have designed the energy functionals for the non-overlapping shapes and derived the governing equations (2.4) with $i = 1$. The models are related to the motion of shapes without considering the grey intensity values of images. In other words, a sequence of images is generated not from the image blending but from the shape warping. In this section, we combine the two methods and suggest the new algorithm for image blending based on warping. The detailed algorithm is explained in the Section 3.1 and the several comments are discussed in Sections 3.2, 3.3 and 3.4.

## 3.1 Algorithm

First of all, we denote given source and target images by $\Phi_0(x, 0)$ and $\Psi_0(x, 0)$, respectively, which are grey scaled. Let $n_0$ be the second lowest intensity value of given images. We define two sets $S_0$ and $T_0$ by

$$\begin{aligned} S_0 &= \{x \in \mathbf{R}^2 : \Phi_0(x, 0) \geq n_0\}, \\ T_0 &= \{x \in \mathbf{R}^2 : \Psi_0(x, 0) \geq n_0\}. \end{aligned}$$

Two signed distance functions $\phi_0(x)$ and $\psi_0(x)$ have positive values in the interior of $S_0$ and $T_0$, negative in $S_0^c$ and $T_0^c$ and zero on each interface $\partial S_0$ and $\partial T_0$. With the signed

distance functions, we obtain the deformation fields $u_0(x,t)$ and $v_0(x,t)$ by solving the PDEs (2.4) with $i=1$. The sequences of images $\Phi_0(x-u_0(x,t),0)$ and $\Psi_0(x-v_0(x,t),0)$ are, respectively, denoted by $\Phi_0(x,t)$ and $\Psi_0(x,t)$. That is, we have

$$\Psi_0(x,t) = \Psi_0(x-v_0(x,t),0),$$
$$\Phi_0(x,t) = \Phi_0(x-v_0(x,t),0).$$

The regions corresponding to the levels $\geq n_0$ for the source and the target become identical in the steady state of (2.4) with $i=1$. However, we may not have the identical shape easily when we only solve (2.4) with $i=1$. If the shape is almost same, then the distance between the source and the target are very small. Hence, much computing time is required to reach the intermediate shape. To have the fast convergence, with some overlapping criterion, we switch over to the equation(2.4) with $i=2$ for overlapping case, which is derived without considering the distance information and solve (2.4) with $i=2$ until the shapes are identical. But, it is not guaranteed that the two images over $n_0$ level coincide. In order to match the rest of the two images over $n_0$ level, we choose the next intensity level $n_1$ which is strictly larger than $n_0$ on the final images $\Phi_0^f(x)$ and $\Psi_0^f(x)$ which are obtained by the steady state vector fields, that is,

$$\Phi_0^f(x) = \lim_{t\to\infty} \Phi_0(x,t),$$
$$\Psi_0^f(x) = \lim_{t\to\infty} \Psi_0(x,t).$$

We secondly denote $\Phi_1(x,0)$ and $\Psi_1(x,0)$ as $\Phi_0^f(x)$ and $\Psi_0^f(x)$, respectively. The values of new signed distance functions $\phi_1(x)$ and $\psi_1(x)$ are assigned for two sets

$$S_1 = \{x \in \mathbf{R}^2 : \Phi_1(x,0) \geq n_1\},$$
$$T_1 = \{x \in \mathbf{R}^2 : \Psi_1(x,0) \geq n_1\}$$

using the same way as for $\phi_0(x)$ and $\psi_0(x)$. Then two deformation fields $u_1(x,t)$ and $v_1(x,t)$ are also obtained. We don't need to apply two deformation fields $u_1(x,t)$ and $v_1(x,t)$ to all pixels in domain $\Omega$ since the regions where intensities of the source image $\Phi_1(x,0)$ and target image $\Psi_1(x,0)$ are less than $n_0$ are already the same. Hence, we preserve the intensity values $< n_0$ until the whole process ends.

The concept of the algorithm is illustrated in Figure 2. After $n_k$ step is finished, we choose the level $n_{k+1}$ which is larger than $n_k$ and calculate the deformation fields $u_{k+1}(x,t)$ and $v_{k+1}(x,t)$ for $k = 0, 1, 2, \cdots, m$ while keeping the regions where the intensities of the source and the target images are less than $n_k$. If $n_m$ is greater than the maximum intensity, then the process is completed.

### 3.2 Interpolations

We consider interpolation methods to generate the image sequence. The intensity values on non-grid points should be calculated because the images of the sequence $\Phi_k(x,t)$ and

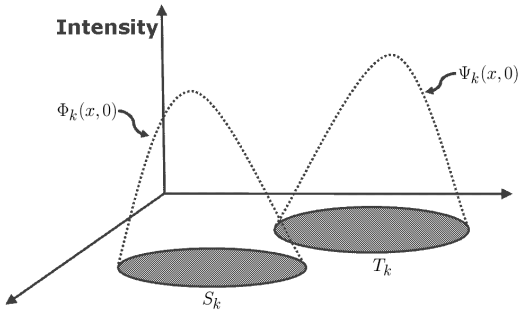


(a)

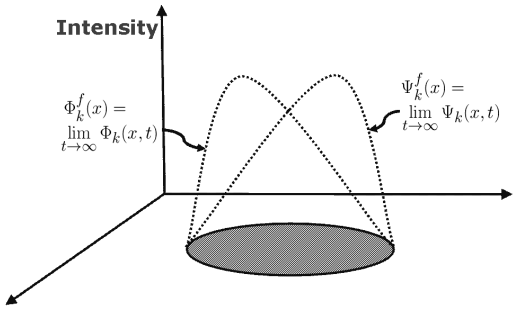


(b)

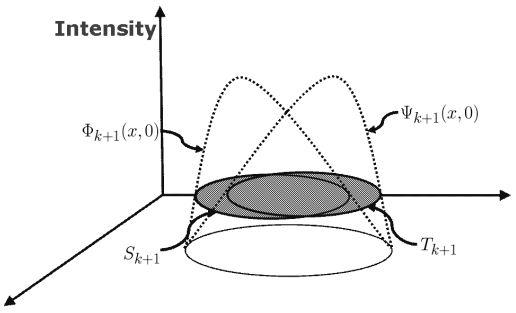


(c)

Figure 2: The algorithm for image blending based on warping: Suppose that the intensity profiles of images are the shape of rounding corn. (a) Choose the initial intensity level $n_k$; the regions over $n_k$ level are the parts with the oblique lines (b) The two shapes at the intensity level $n_k$ become same but the intensity profiles cannot be identical. (c) Choose the next intensity level $n_{k+1}$ that is larger than $n_k$. Do the same process over the level $n_{k+1}$ as before.

$\Psi_k(x,t)$ in the $n_k$ level are obtained by $\Phi_k(x-u_k(x,t),0)$ and $\Psi_k(x-v_k(x,t),0)$. Three methods of interpolation are considered: the bilinear interpolation (BI), the nearest intensity assignment (NIA) and the monotone cubic interpolation (MCI). Let $\xi(x,t) \in \mathbf{R}^2$ be the translated point of the point $x$ by the vector $u(x,t)$, i.e.,

$$\xi(x,t) = x - u(x,t).$$

The simplest striking method is the BI using four grid points near $\xi$. It generates the severe blurring in the image sequence. To avoid blurring, we consider the NIA to assign the intensity value at the closest grid point from $\xi$ to $\xi$. We observe that the image sequence does not have the blurring since the generated images $\Phi_k(x,t)$ and $\Psi_k(x,t)$ have only the intensities sampled in the previous images $\Phi_k(x,0)$ and $\Psi_k(x,0)$, respectively. However, if the magnitudes of the deformation fields are alternatively 0.49 and 0.51 near an edge and the directions are similar, the slight difference between the magnitudes makes the values of intensity non-smooth along the edge even though the previous values are smooth enough. That is, NIA causes zig-zag in the sequence of images. Instead of NIA, we consider the MCI [15] based on the bicubic interpolation with reducing overshooting along the each axis. The image sequence naturally has less zig-zag effect than NIA and less blurring than BI. But, it still causes the noticeable blurring near edges. Therefore, we suggest the weighted sum of NIA and MCI. The typical weight ratio of NIA to MCI is 7:3 or 8:2.

### 3.3 Laplacian weight factor $\alpha$

The Laplacian weight factor $\alpha$ makes the diffusion effect in the deformation fields. The larger $\alpha$ value is in the process, the shorter period of time is taken to obtain the steady deformation fields. For the fixed large $\alpha$, the steady state can be rashly happened before the regions in a level are identical. Then the images in both source and target cannot be updated. In order to get out of stuck, we flexibly reduce the weight factor $\alpha$ by observing the difference between vector fields at the time $t$ and $t+\Delta t$, since the small $\alpha$ value can generate more dynamic transitions in the vector fields.

### 3.4 Stop Criterion

We measure the relative area of symmetric difference of $S_k$ and $T_k$ in $n_k$ level and use the value as the stop criterion to finish the process in the level. The process in $n_k$ level ends when the relative area is less than 1%. Even though we adjust the Laplacian weight factor $\alpha$ in the Section 3.3, the stop criterion in $n_k$ level may not be satisfied when we only use the equations (2.4) with $i=1$. We start to solve (2.4) with $i=1$ derived from the energy functional (2.1) for the non-overlapping case until the relative common area of $S_k$ and $T_k$ in $n_k$ level is over 90%. After that, we solve (2.4) with $i=2$ derived from the energy functional (2.2) for the overlapping case up to satisfying the stop criterion. These are applied for all $n_k$ levels.

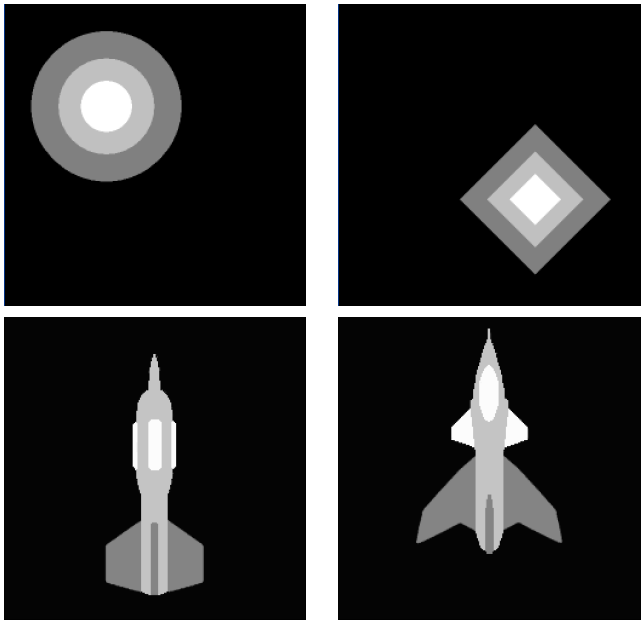

Figure 3: Disk and rectangle (top), dart and airplane (bottom)

## 4 Examples

In this section, we illustrate six examples which consist of 250 by 250 pixels. The first image pairs in Figure 3 are synthetic. We use the disk and the rectangle which are non-overlapped and have simple intensity profiles. We use the synthetic dart and the airplane as more complex shapes. Figure 4 consists of human faces; one is a woman's face that has changed from the inexpressive face to the smiling one and another is a man's face that has changed from the blank face to the angry one. Finally, we illustrate a pair of cups with the clockwise rotation and the Digimon images, namely Koromon and Agumon, which have the relationship of evolution in the animation. Note that handles of cups are non-overlapped.

In Figure 6, the images of the left column are the blending result of the disk and the rectangle. Even though there is no common area of the disk and the rectangle, we can obtain a blending sequence by the proposed method, which gives a dynamic and plausible motion. The right column is the result for the synthetic dart and the airplane. We can see the natural movement, even for the complex geometries.

In Figure 7, we illustrate the blending results of Figure 4. In the woman's face, the natural change of facial expression can be observed in view of the moving of the mouse and eyes. The man's face shows raising left eyebrows which are non-overlapped in the source and the target. Therefore, the pre-existing methods, for examples linear interpolation or level-set approach [2], give the fade-out and the fade-in of the eyebrows and huge blurring occurs in the images of the blending sequence. We can see the dynamic and plausible movement of

Figure 4: Woman's face (top), man's face (bottom)

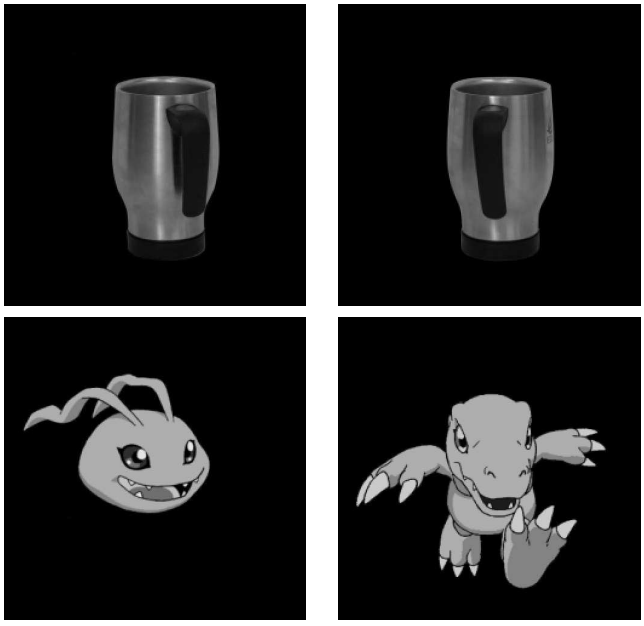

Figure 5: Cup with clockwise rotation (top), Digimon: Koromon (left bottom) and Agumon (right bottom)

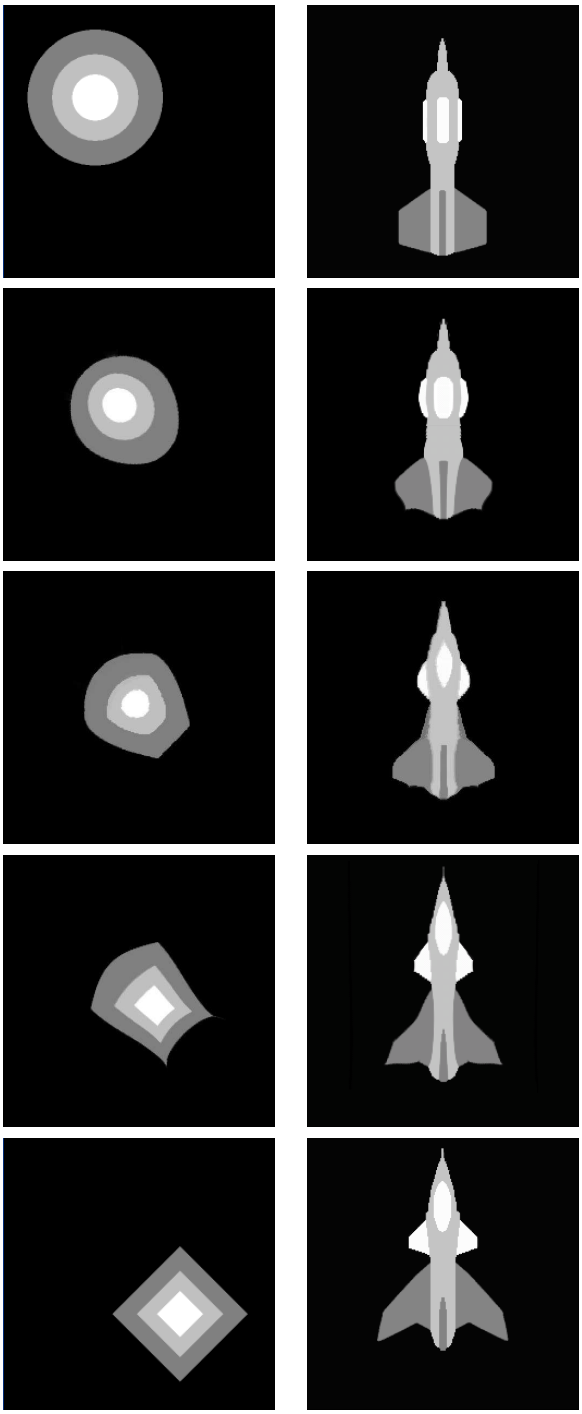

Figure 6: The blending results of Figure 3: The left column is the blending sequence of the disk and the rectangle. The right column is the blending sequence of the dart and the airplane. The images in the third row are the intermediate state.

eyebrows in the image sequence generated by the proposed blending method. It, however, makes a small amount of the zig-zag phenomenon near the shoulder in accordance with the effect of NIA.

In Figure 8, we present the result of cup images which rotate clockwise. The angle of the rotation is enough for handles to be non-overlapped in the source and the target. In the example, we find some troubles in the proposed blending method. The blending sequence has the images whose texture is missing since there is no texture in the right side of the handle in the source. A small amount of the zig-zag effect also occurrs. Despite of the drawbacks, we successfully obtain the images in the blending sequence which contains the rotation of the handle. As the last example, we make the blending sequence with the cartoon images. Agumon is the evolution of Koromon in the animation of DIGIMON ADVENTURE. We embody the intermediate states of the evolution between Koromon and Agumon in the blending sequence. We observe the growing of arms and legs and the moving of the mouse in accordance with the proposed blending method.

## 5 Conclusion

In this paper, we introduced a new blending method based on warping for non-overlapped images. The energy functional in [1] is modified for non-overlapped images without the restriction to take the proper signed distance functions. We derive a system of PDEs for two deformation fields. The blending sequence by the proposed method has the dynamic and plausible motions from the source and the target simultaneously even though the two images are non-overlapped. The two deformation fields reduce the tadpole effects in the blending sequence. We suggest the weighted sum of NIA and MCI in order to get the image intensity on non-grid points. The blending sequence generated by the weighted sum naturally has less zig-zag effect than NIA and less blurring than BI.

## References


[1] W.-H. Liao, A. Khuu, M. Bergsneider, L. Vese, S.-C. Huang, S. Osher, From Landmark Matching to Shape and Open Curve Mathching: A Level Set Approach, Computational and Applied Mathematics (CAM) Technical Reports 02-59, UCLA, 2002.

[2] R.T. Whitaker, A Level Set Approach to Image Blending, IEEE Tran. Image Process. 9(2000) 159-186.

[3] D. Cohen-Or, D. Levin, A. Solomivici, Three-dimensional distance field metamorphosis, ACM Trans. Graph. 17(1998) 117-140.

[4] F.L. Bookstein,Princ ipal warps: thin-plate splines and the decomposition of deformations, IEEE Trans. Pattern Anal. and Mach. Intelligence 11(1989) 567-585.

[5] S.C. Joshi, M.I. Miller, Landmark matching via large deformation diffeomorphisms, IEEE Trans. Image Process. 9(2000) 1357-1370.

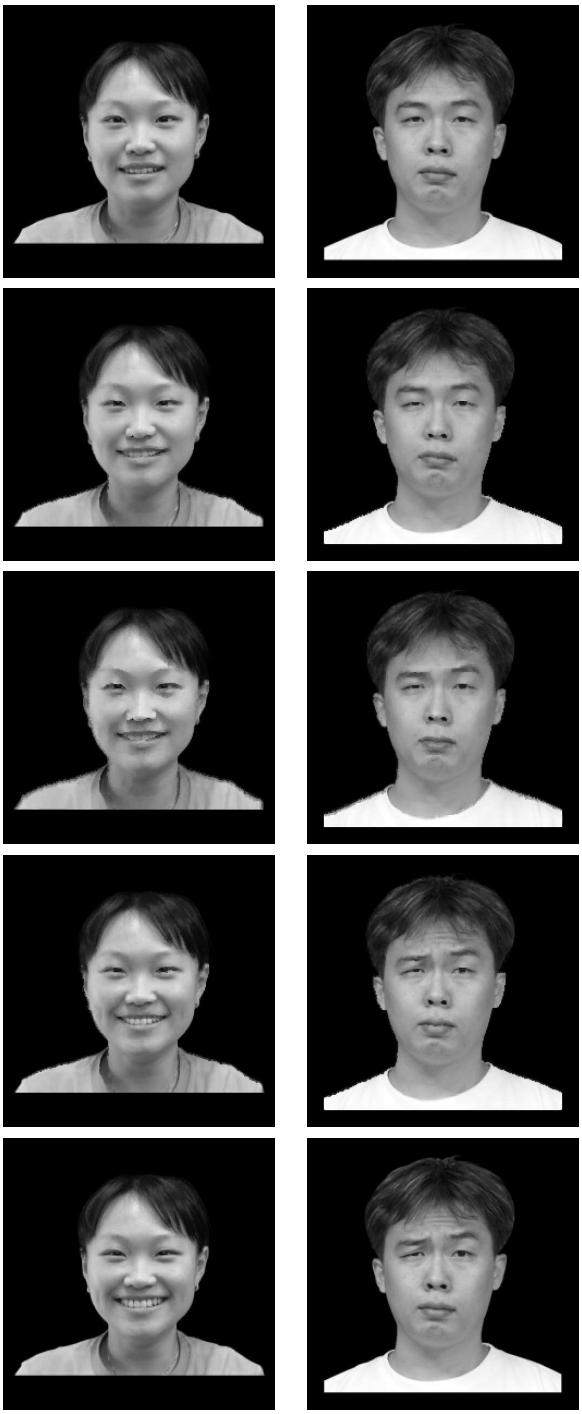

Figure 7: The blending results of Figure 4: The left column is the blending sequence of a woman. The right column is the blending sequence of a man. The images in the third row are the intermediate state.

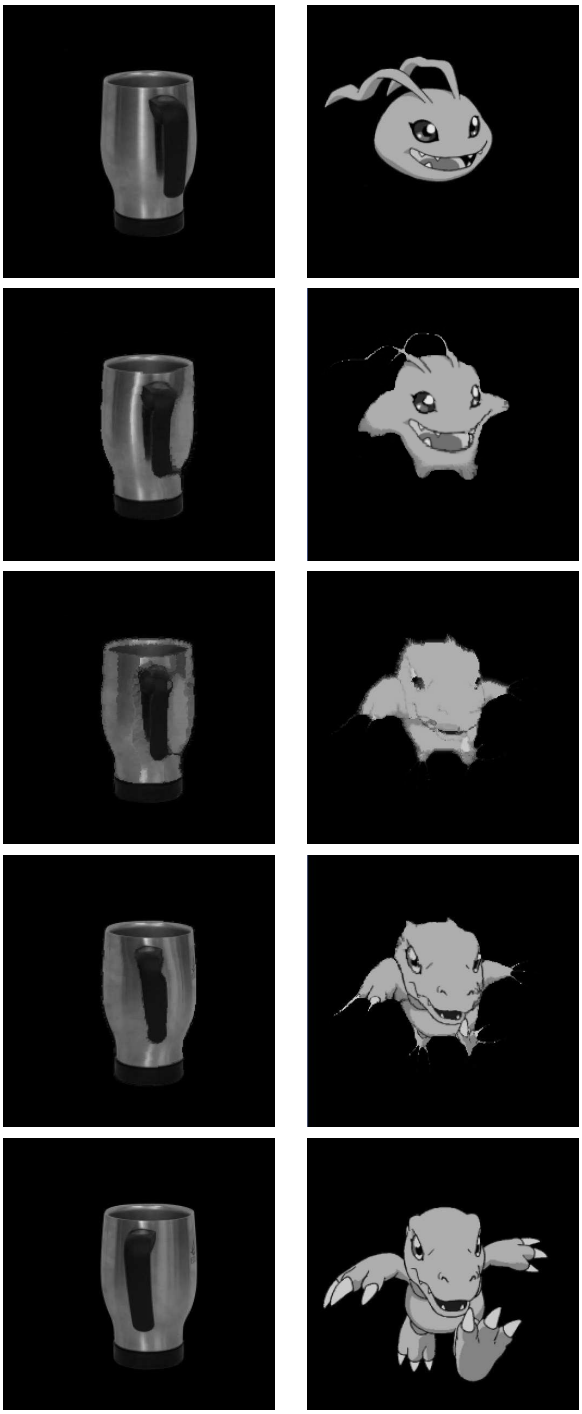

Figure 8: The blending results of Figure 5: The left column is the blending sequence of a cup which rotates clockwise. The right column is Digimon which is an evolution from Koromon to Agumon. The images in the third row are the intermediate state.

[6] S.-Y. Lee, K.-Y. Chwa, S.Y. Shin, G. Wolberg, Image metamorphosis using snake and free-form deformation, in: Proc. ACM SIGGRAPH '95, 1995, pp. 439-448.

[7] B. Fischer, J. Modersitzki, Fast inversion of matrices arising in image processing, Numerical Algorithm 22(1999) 1-11.

[8] B. Fischer, J. Modersitzki, Fast diffusion registration, in: M.Z. Nashed, O. Scherzer (Eds.), Inverse Problems, Image Analysis, and Medical Imaging, Contemporary Mathematics 313, AMS, Providence, 2002, pp. 117-127.

[9] R.T. Whitaker, D. Breen, Level-set models for the deformation of solid objects, in: Implicit Surfaces '98, Eurographics/Siggraph, 1998, pp. 19-35.

[10] S. Henn, K. Witsch, A Variational Image Registration Approach Based on Curvature Scale Space, in: R. Kimmel, N. Sochen, J, Weickert (Eds.), Scale Space and PDE Methods in Computer Vision, LNCS 3459, Springer-Verlag, Berlin, 2005, pp. 143-154.

[11] Y. Amit, A nonlinear variational problem for image matching, SIAM J. Sci. Comput. 15(1994) 207-224.

[12] S. Osher, R. Fedkiw, Level Set Method and Implicit Surface, Applied mathematical science 153, Springer-Verlag, New York, 2003.

[13] J.A. Sethian, Level Set Methods and Fast Marching Methods, second ed., Cambridge University Press, Cambridge, 1999.

[14] B.K.P. Horn, B.G. Shunck, Determining Optical Flow, Atificial intelligence 17(1981) 185-203.

[15] R. Fedkiw, J. Stam, H.W. Jensen, Visual Simulation of Smoke, in: Proc. ACM SIGGRAPH '01, 2001, pp. 15-22.